


Generation and metastability of deep level states in β -Ga₂O₃ exposed to reverse bias at elevated temperatures

Cite as: J. Appl. Phys. **125**, 185706 (2019); <https://doi.org/10.1063/1.5088655>
Submitted: 12 January 2019 . Accepted: 16 April 2019 . Published Online: 14 May 2019

M. E. Ingebrigtsen , A. Yu. Kuznetsov, B. G. Svensson, G. Alfieri, A. Mihaila, and L. Vines



View Online



Export Citation



CrossMark

ARTICLES YOU MAY BE INTERESTED IN

[A review of Ga₂O₃ materials, processing, and devices](#)

Applied Physics Reviews **5**, 011301 (2018); <https://doi.org/10.1063/1.5006941>

[Impact of proton irradiation on conductivity and deep level defects in \$\beta\$ -Ga₂O₃](#)

APL Materials **7**, 022510 (2019); <https://doi.org/10.1063/1.5054826>

[Iron and intrinsic deep level states in Ga₂O₃](#)

Applied Physics Letters **112**, 042104 (2018); <https://doi.org/10.1063/1.5020134>



Lock-in Amplifiers

Zurich Instruments

Watch the Video 

Generation and metastability of deep level states in β -Ga₂O₃ exposed to reverse bias at elevated temperatures

Cite as: J. Appl. Phys. **125**, 185706 (2019); doi: [10.1063/1.5088655](https://doi.org/10.1063/1.5088655)

Submitted: 12 January 2019 · Accepted: 16 April 2019 ·

Published Online: 14 May 2019



View Online



Export Citation



CrossMark

M. E. Ingebrigtsen,^{1,a)} A. Yu. Kuznetsov,¹ B. G. Svensson,¹ G. Alfieri,² A. Mihaila,² and L. Vines¹

AFFILIATIONS

¹University of Oslo, Pb 1048 Blindern, 0316 Oslo, Norway

²ABB Corporate Research, Segelhofstrasse 1K, 5405 Baden-Dättwil, Switzerland

^{a)}m.e.ingebrigtsen@smn.uio.no

ABSTRACT

An intriguing phenomenon of electrically active defect generation is observed in homoepitaxial β -Ga₂O₃ films exposed to reverse bias at elevated temperatures. In particular, heating samples up to 675 K in the course of deep level transient spectroscopy measurements, i.e., with the reverse bias and voltage pulsing applied, resulted in the generation of three new levels at ~ 1 , ~ 1.5 , and ~ 2 eV below the conduction band edge (labeled as E3*, E5, and E6). The corresponding defects exhibit different thermal stabilities; E5 and E6 show stability, while E3* demonstrates a remarkable metastability—it can be generated, annealed out, and regenerated in the course of sequential temperature cycles. Combining a number of annealing tests and using different types of epitaxial materials, the levels were systematically investigated, and the most credible scenario behind the phenomenon is the evolution of already existing defect configurations provoked by the applied temperature and bias.

Published under license by AIP Publishing. <https://doi.org/10.1063/1.5088655>

INTRODUCTION

The research interest in semiconducting gallium oxide in its so-called β -form (β -Ga₂O₃) has been significantly renewed over the recent years. This was motivated by the prospects of its use in such applications as power electronics, UV devices, and passivating or transparent conductive oxide for solar cells. Among the other materials used for these applications, β -Ga₂O₃ exhibits one of the largest bandgaps around 4.8 eV.^{1,2} The n-type conductivity in β -Ga₂O₃ is readily achieved in the range of 10^{16} – 10^{19} cm⁻³ using Si or Sn as dopants,³ while semi-insulating substrates can be produced by incorporating compensating acceptors such as Fe, Mn, and Mg.⁴ Another often quoted technological advantage of β -Ga₂O₃ as compared to its competitors (e.g., SiC and GaN) is the availability of melt growth synthesis.^{5–7} This is relevant for manufacturing devices directly in a bulk material as well as providing substrates for subsequent homoepitaxial growth. Indeed, epitaxial films of high crystalline quality and with low concentrations of residual impurities have been demonstrated using molecular beam epitaxy (MBE) and halide vapor phase epitaxy (HVPE).^{8,9} Notably, β -Ga₂O₃ synthesis without intentional doping is found to yield an

n-type material, commonly attributed to residual Si or H impurities.² Schottky contacts with high energy barriers and low ideality factors can be formed by several high work function metals, including Au, Ni, Pt, and Cu, on β -Ga₂O₃.^{10–14} Recently, ten orders of magnitude rectification was reported using Pt contacts,¹⁵ and optimizing the edge termination using field-plates has allowed a record-high breakdown voltage of 1076 V with the same material.¹⁶

The understanding of the localized electronic states in the bandgap of β -Ga₂O₃ is still limited, although pioneering experimental studies on bulk samples have recently been extended toward more detailed analysis of both bulk and thin-film materials. Using deep level transient spectroscopy (DLTS) on Czochralski grown material, Irmscher *et al.*¹⁰ reported three levels at 0.55, 0.74, and 1.04 eV below the conduction band edge (E_C), labeled E1, E2, and E3, respectively. In edge-defined film-fed grown (EFG) samples, Zhang *et al.*¹⁷ observed, in addition to E1–E3, two other levels deeper in the bandgap applying optical excitation, particularly at 2.16 and 4.4 eV below E_C . Further, a fourth level was reported in EFG samples at ~ 1.48 eV below E_C and was labeled E4.¹⁸ Moreover, Fe has been recognized as the cause of the most

prominent level in the bulk material (E2), whereas another closely located level (E2*) was found to be generated by proton irradiation.¹⁹ Gao *et al.* have employed oxygen plasmas and forming gas anneals, as examples of oxidizing and reducing treatments, for the purpose of varying the intrinsic point defect balance in β -Ga₂O₃.²⁰ Combining the data from photovoltage spectroscopy and cathodoluminescence spectroscopy, a number of localized electronic states were reported^{2,21} and set in the context of the theoretical predictions for oxygen and gallium vacancies.

In turn, *ab initio* calculations of defect configurations in β -Ga₂O₃ have contributed to the understanding of their electronic properties too, although the data are not fully consistent. In the monoclinic structure of β -Ga₂O₃, there are two different cation environments; following the notation given in Ref. 21, Ga(I) is tetrahedrally coordinated and Ga(II) is octahedrally coordinated. Varley *et al.* predicted that the vacancies on these sites act as deep acceptors at 1.62 and 1.83 eV below E_C for V_{Ga}^I and V_{Ga}^{II}, respectively.²¹ However, a more recent theoretical treatment by Deák *et al.* placed these (-2/-3) transition states at 0.67 eV and 1.16 eV from E_C, for V_{Ga}^I and V_{Ga}^{II}, respectively.²² In turn, the oxygen sublattice has three different environments, where O(I) and O(II) are threefold coordinated, while O(III) exhibits fourfold coordination. According to Varley *et al.*, oxygen vacancies were predicted to be deep donors with (0/2) transition states at ~1.6, 2.2, and 1.3 eV from E_C, for V_O^I, V_O^{II}, and V_O^{III}, respectively.² Again, these values were contested by Deák *et al.*, computing significantly higher values, specifically 2.10, 2.68, and 1.95 eV from E_C, for the same order of the O vacancy configurations.

In the present paper, we report a new set of DLTS data emphasizing the measurements above room temperature, allowing observation of deep traps down to ~2 eV from the E_C. The data were collected from epitaxial thin films of β -Ga₂O₃ grown by MBE and HVPE having different background impurity levels and surface orientations. An intriguing behavior was observed in a part of the samples; the reverse bias application in combination with high temperature (>600 K) resulted in the generation of deep levels labeled as E3*, E5, and E6. The focus of the paper is on documenting electronic properties of these new levels, specifically including depth profiling of E3*, as well as discussing possible origins of the defects.

EXPERIMENTAL

The MBE and HVPE homoepitaxial films were produced by Tamura corp. on substrates with (010) and (001) surface orientations, respectively. *In situ* Sn doping of the substrates provides charge carrier concentrations (n_e) of $\sim 10^{18}$ cm⁻³ and thus a low-resistive foundation for the films. Notably, in the 2 μ m thick MBE film, a substantial variation in n_e across the sample was observed, ranging from $\sim 3 \times 10^{16}$ cm⁻³ to much lower values resulting in

complete depletion of the film in a corresponding diode already at zero bias. Thus, in order to make reliable measurements, most of the capacitance data as reported in the rest of the paper were collected from the diodes exhibiting charge carrier concentrations $\sim 3 \times 10^{16}$ cm⁻³, if not otherwise stated. The HVPE epitaxial films were 10 μ m thick with $n_e = 5\text{--}8 \times 10^{16}$ cm⁻³. For the diode preparation, the wafers were laser cut to 5 \times 5 mm and cleaned in ultrasonically agitated baths of sequentially acetone (2 min), isopropanol (10 min), and water (5 min) to remove organic contaminants. E-beam deposition of Ni was used to manufacture Schottky contacts that exhibited suitable properties for the DLTS characterization.¹⁸ Circular Ni contacts with radii 100, 240, and 400 μ m were deposited through a shadow mask on the wafers using e-beam evaporation. A stack of Ti/Al was applied to the back of the wafers to serve as an ohmic contact, also using e-beam evaporation. Initial quality assurance of the Schottky contacts was done with *IV* measurements, and Capacitance-Voltage (CV) was performed to map the charge carrier concentrations across the diodes on the wafers. The DLTS data were collected in the temperature range of 200–675 K, while the emphasis was on the above room temperature part of the range allowing the characterization of quite deep states, down to ~2 eV below E_C. A major part of the data were collected using 8 V reverse bias (V_r) with pulsing to 1 V, whereas other conditions were chosen to investigate the field dependence, as will be specified in the corresponding section. The depth profiling of the traps was carried out with a quiescent reverse bias of 15 V at a constant temperature corresponding to the peak position, by recording the DLTS signal as a function of gradually increasing filling pulses. The DLTS capacitance response was recorded using an HP 4280A capacitance meter, and analysis of the transients was done using lock-in and GS4 weighting functions, in rate windows from 20 ms⁻¹ to 2560 ms⁻¹. The 640 ms⁻¹ rate window was used for comparing different measurements herein. For mapping concentrations of the extrinsic impurities in the films, secondary ion mass spectrometry (SIMS) was performed using the Cameca IMS7f tool. In general, we observed quite homogeneous impurity depth profiles, as well as the lateral homogeneity across the samples, e.g., when measuring directly on the Schottky diodes used for the DLTS characterization. Specifically, the concentrations of impurities detected in the MBE and HVPE samples are summarized in Table I.

RESULTS

Figure 1 shows typical examples of the DLTS spectra for the MBE and HVPE samples, where the y-axis estimates the deep level concentration for the corresponding peaks. The data were collected during both heating and cooling of the samples, with the heating and cooling rates of ~2 K/min. Normally, in DLTS measurements, the data collected in either cooling or heating stages are nearly

TABLE I. Concentrations of extrinsic impurities in the MBE and HVPE samples as recorded by SIMS and reported in cm⁻³.

B	Al	Si	In	Sn	Mg	Cr	Fe
$\sim 1 \times 10^{17}$	5×10^{14}	1.8×10^{17}	$\sim 1 \times 10^{15}$	4×10^{16}	$\sim 1 \times 10^{14}$	$\sim 1 \times 10^{14}$	$\sim 1 \times 10^{15}$
$< 1 \times 10^{14}$	8×10^{15}	2×10^{17}	5×10^{14}	2.5×10^{13}	1×10^{15}	7×10^{14}	$< 1 \times 10^{15}$

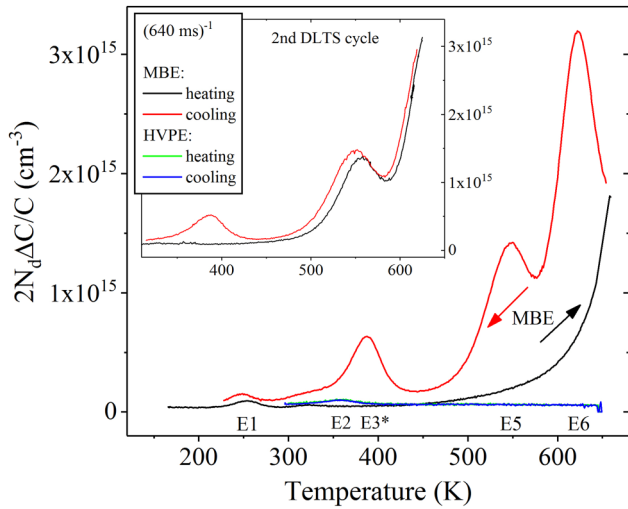


FIG. 1. Examples of the DLTS spectra collected during heating and cooling of the samples. Importantly, for the HVPE diodes, the heating and cooling data practically coincide, as is the expectation for DLTS measurements. Meanwhile, the MBE diode data reveal defect generation during the measurement. Labeling of E1 and E2 is in accordance with the literature, while E3*, E5, and E6 are newly observed in this work. The inset shows the data collected from the second DLTS cycle on the MBE diode.

identical, as is the case in Fig. 1 for the HVPE samples. Nearly identical data from heating and cooling were also observed in bulk β -Ga₂O₃; see, e.g., Refs. 18 and 19. On the other hand, the comparison of the heating and cooling data as collected from the MBE sample shows a dramatic difference. The black line in Fig. 1 represents the DLTS signal upon the first heating attempt, while the red line represents the signal from the subsequent cooling stage, as indicated by the arrows. From the comparison of these two sets of data, it is evident that the heating of the MBE diodes with a reverse bias applied, resulted in the generation of defects in the high-temperature part of Fig. 1. Specifically, three new deep levels are revealed in the cooling stage in Fig. 1, and these are labeled E3*, E5, and E6. Subsequent measurements reveal that the thermal stability of these DLTS signatures is not identical. After generating E3*, E5, and E6 in the first measurement cycle, E5 and E6 remain through to the second measurement cycle as is evident from the inset in Fig. 1. Importantly, between the two measurement cycles, the sample was annealed at 650 K in the sample holder without applying bias. This was done in a similar temperature cycle up to

650 K with ~ 2 K/min. Intriguingly, this annealing removed the E3* signature, so it is not observable at the heating stage of the second cycle, although it does reappear in the second cooling stage.

Table II summarizes the electronic properties of the traps observed in Fig. 1. The level labeled as E1 (here and in the literature) exhibits characteristics similar to those reported previously.^{10,17,18} The properties of E2 observed in the HVPE sample are also consistent with the literature.¹⁹ Both these levels are seen at low concentrations in our samples and are taken out of consideration in the rest of our analysis. Instead, the focus will be on the newly observed E3*, E5, and E6 levels. Of these, the level labeled E3* appears in Fig. 1 in the range of previously reported E3. However, since the generation and thermal stability of E3* in Fig. 1 is different from that of E3 in the literature, a discrimination in the labeling is made. Similar arguments hold for the level labeled E5 in Fig. 1, appearing in the range of previously reported E4 and E4*.^{18,19,23,24} Nevertheless, since the properties of E5 differs from those of E4 and E4*, we propose to make a distinction here too. The range of E6 in Fig. 1 was not investigated previously and labeling here is unambiguous.

Besides the observations in Fig. 1, it is also worth noting that preheating of the MBE diodes up to 675 K without applying the bias does not introduce E3*, E5, or E6 levels in the samples. Furthermore, the data depicted in Fig. 1 are reproducible across a large number of MBE diodes on the same sample, implying that only elevating the temperature up to 675 K is not sufficient for the generation of E3*, E5, and E6. Additional influencing factors are the reverse bias and pulsing occurring during the DLTS measurements only to the diode being measured. However, before exploring these effects, Fig. 2 represents more detailed data on the thermal generation properties of E3*, E5, and E6. Herein, we performed sequential DLTS measurements, with the first done from temperatures below the E3* peak, up to 500 K and returning back to the initial temperature. Then, the following DLTS cycles were performed with increasing the upper temperature limit in steps of 25 K. This was done on a virgin diode, i.e., without previously generated deep levels. On top of a gradual onset of the DLTS signal, the E3* and E5 peaks are not revealed before reaching the 625 K step. For E6, the onset trend at the lower temperature steps indicates its earlier generation; see Fig. 2. However, since the E6 peak is outside of the measurement range for the lower temperature steps, we cannot conclude categorically on the temperature required for the E6 generation.

The data shown in Figs. 3 and 4 extend our argument that the reverse bias conditions also—in addition to the temperature—influence the defect generation, in particular studying the E3* level. Figure 3 depicts the depth profiles of the E3* peak, done after three

TABLE II. Energy positions ($E_C - E_t$) and apparent capture cross sections (σ_n) for the deep levels observed in this work. Note, the range for E3* is included due to extra measurements done to evaluate the field dependency (discussed in connection with Fig. 4). Additionally, the larger uncertainties in E5 and E6 values are due to wider peaks challenging the accuracy at higher temperatures.

	E1	E2	E3*	E5	E6
$E_C - E_t$ (eV)	0.56 ± 0.03	0.78 ± 0.04	$0.92\text{--}1.05 \pm 0.05$	1.5 ± 0.15	1.8 ± 0.2
σ_n (cm ²)	$0.3\text{--}5 \times 10^{-13}$	$0.2\text{--}1.2 \times 10^{-15}$	$0.2\text{--}6 \times 10^{-13}$	$10^{-14}\text{--}10^{-11}$	$10^{-12}\text{--}10^{-9}$

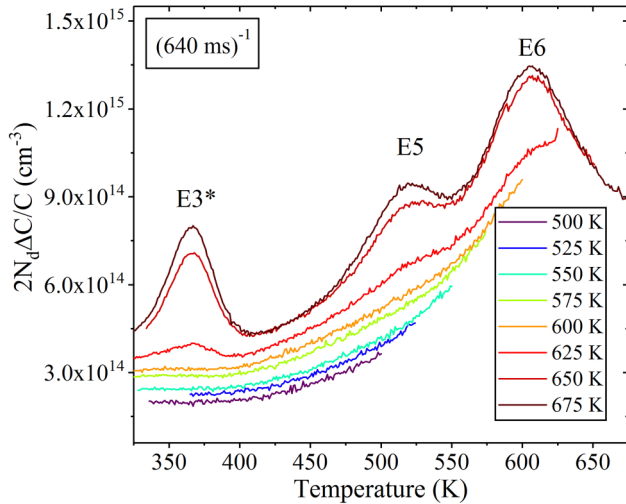


FIG. 2. Sequential DLTS measurements revealing temperature generation limits for E3*, E5, and E6.

different high-temperature DLTS cycles with reverse bias of 8, 12, and 16 V, respectively, but all with pulsing to 1 V. The profiles themselves are recorded at the peak temperature, evidently (from data in Fig. 2) not affecting the E3* generation. First, Fig. 3 reveals strongly asymmetric depth profiles, indicating the maximum E3* generation to occur in the region close to that with the maximum applied electric field. Second, increasing the reverse bias of the intermediary DLTS measurements increases the material volume

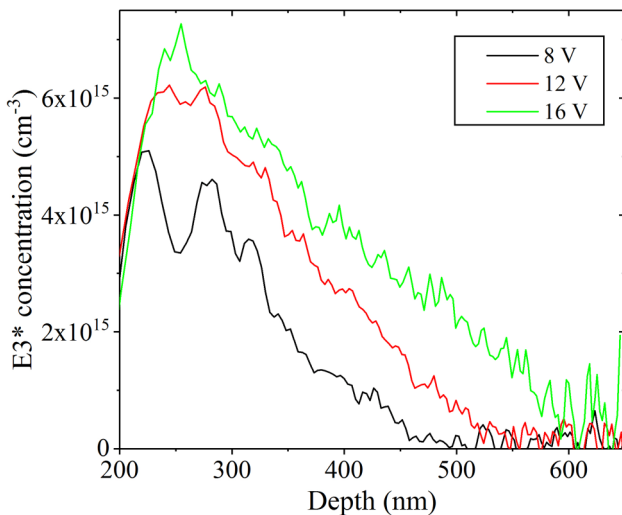


FIG. 3. E3* concentration vs depth profiles as collected at the peak temperature of the 640 ms⁻¹ rate window. The profiles were recorded on one diode after the DLTS measurements with 8, 12, or 16 V reverse bias at up to 650 K (called intermediary DLTS measurements in the text).

affected by the electric field. Indeed, as seen in Fig. 3, the E3* generation deeper in the material scales with the application of the higher reverse bias. In other words, the form of the depth profiles in Fig. 3 correlates with the depletion region properties occurring in the intermediary DLTS measurements.

Another reason for doing the measurements as a function of the reverse bias was to monitor the peak signature response; see Fig. 4. It is evident from Fig. 4 that the E3* peak position shifts toward lower temperatures with increasing the reverse bias. Notably, increasing the reverse bias is proportional to increasing the electric field (*E*) in the depletion region, resulting in steeper band bending at the Schottky contact. As such, the potential well of the defect is distorted, which causes a lowering of the barrier and thus enhancing the electron emission. As a result, the energy position of the electronic level observed through DLTS is lowered. This phenomenon is known as the Poole-Frenkel effect, and a linear relation between the energy level position and the square root of the electric field is expected.²⁵ This relation is plotted in the inset in Fig. 4, assuming a constant capture cross section (σ_n). Since only donorlike states exhibit this field-enhanced emission in n-type material, we conclude that E3* is a donor state. Notably, the variation in the E3* peak amplitude in Fig. 4 is related to the fact of probing different depths when varying the bias so that the signal decreases in accordance with the profiles in Fig. 3.

Similar to that for E3*, profiling measurements were performed on E5 and revealed a similar trend of E5 generation scaling with the volume of the depletion region (not shown). Neither E5 nor E6 showed significant systematic changes in the peak position as a function of the applied voltage, i.e., the Poole-Frenkel effect was not observed. Thus, the question on whether these defects have donor or acceptor nature remains.

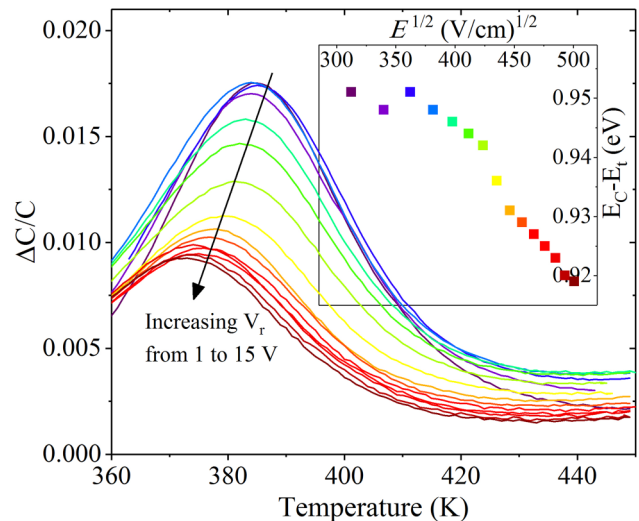


FIG. 4. E3* peak position shifts as a function of applied bias. The field dependence is deduced from the shifting peak position and is plotted in the inset following Poole-Frenkel formalism. The color legends in the inset and the main panel are the same. Note that the initial E3* generation occurred during a DLTS cycle with 8 V reverse bias.

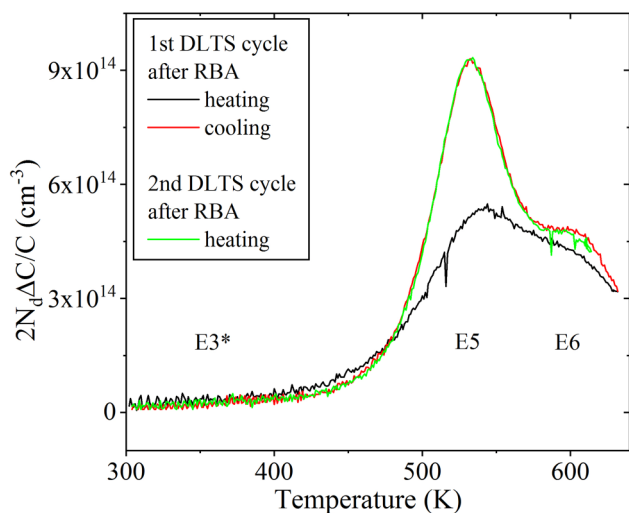


FIG. 5. Examples of the DLTS spectra collected after the reverse bias anneal resembling the conditions of the heating step in the DLTS cycle in Fig. 1.

Finally, Fig. 5 shows the DLTS spectra collected from the MBE diode after annealing with 8 V reverse bias applied, called reverse bias annealing (RBA) below. The RBA was carried out by cycling the temperature in a similar manner as that during the DLTS measurements and always keeping the bias on the diode, meaning heating and cooling to the maximum temperature at a rate of 2 K/min. Basically, only the filling pulses were absent as compared to the conditions of the DLTS measurements. The first DLTS measurement after the RBA (black line in Fig. 5) reveals the E5 generation and to a smaller extent the E6 generation occurred during RBA (compare the data in Figs. 1 and 5). Nevertheless, additional generation occurs in the DLTS measurement too, as revealed by the higher E5 signal in the cooling step of the first measurement cycle. This suggests that the pulsing of the DLTS measurement plays a role in the generation properties of at least the E5 level. It should be noted that in the RBA experiment, we used the diodes exhibiting substantially lower charge carrier concentration, so the volume probed in Fig. 5 is much bigger compared to that in Fig. 1. As such, if E3* piles up in the vicinity of the interface, as may be speculated from the asymmetry of the profiles in Fig. 3, the absence of E3* in Fig. 5 may be attributed to its comparatively lower fraction in samples with lower carrier concentration. In any case, even though the detailed picture of the defect generation occurring during RBA and during the DLTS measurement cycles is different, the fundamental conclusion is the same—the combination of the reverse bias and high-temperature results in the defect generation not otherwise observable in the same samples.

DISCUSSION

DLTS is known to be a powerful technique to monitor electronic properties of deep localized states in semiconductors. However, no information on the microscopic origin of the

electronic levels can be obtained directly. Simplistically speaking, the only way to proceed with experimental identification of the DLTS peaks is to collect data from a set of samples known to exhibit some systematic variations and analyze whether these parameters correlate with the intensity of the DLTS peaks. Such variations can be in impurity or intrinsic defect concentrations, sample orientation, and/or sample treatments. In addition, with significantly improved accuracy of the theoretical predictions, the comparison of the DLTS data with the results of *ab initio* simulations can be instructive too. In the discussion below, we use the combination of these two approaches in order to interpret the data in Figs. 1–5.

In the first approximation, deep levels are caused by point defects of either intrinsic or extrinsic origin; however, extended defects like complexes or even dislocations can exhibit mid-bandgap electronic signatures too.^{26,27} In more complex semiconductors, such as β -Ga₂O₃, with a number of inequivalent lattice sites, the probability of building complexes may only increase. Generally speaking, judging from our observations, the origin of E3*, E5, and E6 may be due to either (i) generation of new intrinsic point defects, (ii) in-diffusion of the mobile defects from the bulk of the sample, or (iii) changing the configuration of already existing defects. Importantly, whatever mechanism of (i)–(iii) is working, it occurs only in the depletion region of the diode, stimulated by the elevated temperature and applied reverse bias. Considering (i), at the first glance, the positions of E5 and E6 match well with the positions of V_{Ga}^{I} and $V_{\text{Ga}}^{\text{II}}$, respectively, as predicted by Varley *et al.*²¹ This hypothesis is further supported by the low migration barriers and formation energies in accordance with calculations in Ref. 21. As a result, V_{Ga}^{I} and $V_{\text{Ga}}^{\text{II}}$ may be mobile at the temperatures of our experiments, matching the generation as observed in Figs. 1, 2, and 5. However, Deák *et al.*²² more recently predicted that V_{Ga}^{I} and $V_{\text{Ga}}^{\text{II}}$ exhibit shallower electronic states compared to our observation. Additionally, and even more critical for hypothesis (i), is the fact that the generation of E3*, E5, and E6 occurs only in a part of the studied samples, specifically in the MBE grown samples, while the HVPE samples do not support the trend (being essentially the same material, with similar carrier concentrations). Thus, assigning E3*, E5, and/or E6 to be newly generated intrinsic point defects is ambiguous. Further, hypothesis (ii), i.e., the in-diffusion of defects from the bulk into the depletion region, seems to be unlikely too. First, because the diffusion in the bulk might occur independently of the bias applied to the diode, the control annealing-only experiments do not reveal new levels. Second, as checked by SIMS (not shown), no impurity redistribution upon the DLTS measurements was observed, within the accuracy of SIMS. However, even though impurity redistribution was not detected, the role of extrinsic defects cannot be totally neglected, considering a possibility for impurities to occur in different lattice configurations. As discussed in the literature—e.g., correlating Fe and E2 contents in bulk β -Ga₂O₃¹⁹—the deviation from one-to-one correlation here indicated that Fe occurs in other configuration(s) in addition to that giving rise to E2. Generalizing the argument, the observation of a homogeneous chemical impurity depth profile does not exclude variations in the profiles of specific defect configurations, e.g., potentially matching the observation in Fig. 3. This consideration bridges to hypothesis (iii) meaning that the high temperature in combination with the reverse bias can change

the configuration of a pre-existing defect and, as such its electrical manifestation in the bandgap. The process may occur either by simply moving an impurity from one lattice site to another or reconstructing bigger defect complexes. Indeed, the only two substantial differences between the MBE and HVPE samples are (010) vs (001) orientations and residual impurity backgrounds, making hypothesis (iii) most reliable. Additionally, the pulsing conditioning of the DLTS measurement may facilitate transitions from one configuration to another. For example, consider having a defect deeper in the bandgap than we can observe with our DLTS setup, but likely to be available and observed, for instance, by capacitance spectroscopy with optical excitation and cathodoluminescence,^{17,20} and as predicted by theory.^{21,22} In the course of the DLTS measurement or RBA treatment, such a defect may change the configuration and reveal new level(s) as observed in Figs. 1–5. Importantly, the trends of relatively low-temperature generation and removal of deep levels were recently observed in β -Ga₂O₃ upon proton irradiation too,²⁴ suggesting that defect reactions with relatively low activation barriers indeed occur in this material, making it a very interesting “laboratory” to study defects in semiconductors.

CONCLUSIONS

An intriguing phenomenon of electrically active defect generation was observed in homoepitaxial β -Ga₂O₃ films exposed to reverse bias at elevated temperatures. In particular, heating up to 675 K in the course of the DLTS measurements, i.e., with reverse bias and voltage pulsing applied, resulted in the generation of three new levels at ~ 1 , ~ 1.5 , and ~ 1.8 eV below E_C (labeled E3*, E5, and E6, respectively). Notably, preheating of the samples under constant reverse bias reveals new levels already at the heating step of the DLTS measurement cycle. However, at least for E5, the corresponding peak intensity doubles in the cooling set of the data, discriminating the contribution of the voltage pulsing in the preheated samples. Importantly, anneals without biasing showed no influence on subsequent DLTS spectra, confirming that the temperature activation alone is not sufficient to generate these levels. Further, the argument of the field-assisted process was confirmed by the E3* depth profiling data revealing its generation within the depletion region only. Meanwhile, the observed defects exhibit different thermal stabilities; E5 and E6 show stability, while E3* demonstrates a remarkable metastability—it can be generated, annealed out, and regenerated in the course of sequential temperature cycles. Interestingly, E3* shows donorlike behavior, prominently varying its energy position as a function of the electric field in accordance with the Poole–Frenkel formalism. Importantly, the bias and temperature treatments used in this work were sufficient to induce the levels in the MBE epitaxial films, while the HVPE material remained unaffected. The prime focus of this work was to document the properties of E3*, E5, and E6 electronic levels, and more data must be collected in order to conclude on the microscopic origin of the observed electronic signatures. However, taking into account the fact that not all samples exhibit similar behavior, the most credible scenario behind the phenomenon is the evolution of already existing defect configurations provoked by the applied temperature and bias.

ACKNOWLEDGMENTS

The Research Council of Norway is acknowledged for the support through the Synknøyt and FriPro programs (Project Nos. 228578, 239895, and 251131), and the Norwegian Micro- and Nano-Fabrication Facility (Project No. 197411/V30). Financial support from the University of Oslo and UiO:Energy through the GOPEF Project is acknowledged too.

REFERENCES

- ¹H. H. Tappin, *Phys. Rev.* **140**(1A), A316–A319 (1965).
- ²J. B. Varley, J. R. Weber, A. Janotti, and C. G. Van de Walle, *Appl. Phys. Lett.* **97**(14), 142106 (2010).
- ³E. G. Villora, K. Shimamura, Y. Yoshikawa, T. Ujiie, and K. Aoki, *Appl. Phys. Lett.* **92**(20), 202120 (2008).
- ⁴M. Higashiwaki, K. Sasaki, H. Murakami, Y. Kumagai, A. Koukitsu, A. Kuramata, T. Masui, and S. Yamakoshi, *Semicond. Sci. Technol.* **31**(3), 034001 (2016).
- ⁵H. Aida, K. Nishiguchi, H. Takeda, N. Aota, K. Sunakawa, and Y. Yaguchi, *Jpn. J. Appl. Phys.* **47**(11R), 8506 (2008).
- ⁶E. G. Villora, K. Shimamura, Y. Yoshikawa, K. Aoki, and N. Ichinose, *J. Cryst. Growth* **270**(3–4), 420–426 (2004).
- ⁷Z. Galazka, R. Uecker, K. Irmscher, M. Albrecht, D. Klimm, M. Pietsch, M. Brützm, R. Bertram, S. Ganschow, and R. Fornari, *Cryst. Res. Technol.* **45**(12), 1229–1236 (2010).
- ⁸K. Sasaki, M. Higashiwaki, A. Kuramata, T. Masui, and S. Yamakoshi, *J. Cryst. Growth* **378**(0), 591–595 (2013).
- ⁹H. Murakami, K. Nomura, K. Goto, K. Sasaki, K. Kawara, Q. T. Thieu, R. Togashi, Y. Kumagai, M. Higashiwaki, A. Kuramata, S. Yamakoshi, B. Monemar, and A. Koukitsu, *Appl. Phys. Express* **8**(1), 015503 (2015).
- ¹⁰K. Irmscher, Z. Galazka, M. Pietsch, R. Uecker, and R. Fornari, *J. Appl. Phys.* **110**(6), 063720 (2011).
- ¹¹R. Suzuki, S. Nakagomi, Y. Kokubun, N. Arai, and S. Ohira, *Appl. Phys. Lett.* **94**(22), 222102 (2009).
- ¹²K. Sasaki, M. Higashiwaki, A. Kuramata, T. Masui, and S. Yamakoshi, *IEEE Electron. Device Lett.* **34**(4), 493–495 (2013).
- ¹³J. Yang, S. Ahn, F. Ren, S. J. Pearton, S. Jang, J. Kim, and A. Kuramata, *Appl. Phys. Lett.* **110**(19), 192101 (2017).
- ¹⁴H. Fu, H. Chen, X. Huang, I. Baranowski, J. Montes, T. Yang, and Y. Zhao, *IEEE Trans. Electron Devices* **65**(8), 3507–3513 (2018).
- ¹⁵Q. He, W. Mu, H. Dong, S. Long, Z. Jia, H. Lv, Q. Liu, M. Tang, X. Tao, and M. Liu, *Appl. Phys. Lett.* **110**(9), 093503 (2017).
- ¹⁶K. Konishi, K. Goto, H. Murakami, Y. Kumagai, A. Kuramata, S. Yamakoshi, and M. Higashiwaki, *Appl. Phys. Lett.* **110**(10), 103506 (2017).
- ¹⁷Z. Zhang, E. Farzana, A. R. Arehart, and S. A. Ringel, *Appl. Phys. Lett.* **108**(5), 052105 (2016).
- ¹⁸M. E. Ingebrigtsen, L. Vines, G. Alfieri, A. Mihaila, U. Badstübner, B. G. Svensson, and A. Yu. Kuznetsov, *Mater. Sci. Forum* **897**, 755–758 (2017).
- ¹⁹M. E. Ingebrigtsen, J. B. Varley, A. Y. Kuznetsov, B. G. Svensson, G. Alfieri, A. Mihaila, U. Badstübner, and L. Vines, *Appl. Phys. Lett.* **112**(4), 042104 (2018).
- ²⁰H. Gao, S. Muralidharan, N. Pronin, M. R. Karim, S. M. White, T. Asel, G. Foster, S. Krishnamoorthy, S. Rajan, L. R. Cao, M. Higashiwaki, H. V. Wenckstern, M. Grundmann, H. Zhao, D. C. Look, and L. J. Brillson, *Appl. Phys. Lett.* **112**(24), 242102 (2018).
- ²¹J. B. Varley, H. Peelaers, A. Janotti, and C. G. V. de Walle, *J. Phys. Condens. Matter* **23**(33), 334212 (2011).
- ²²P. Deák, Q. Duy Ho, F. Seemann, B. Aradi, M. Lorke, and T. Frauenheim, *Phys. Rev. B* **95**(7), 075208 (2017).
- ²³A. Y. Polyakov, N. B. Smirnov, I. V. Shchemerov, E. B. Yakimov, J. Yang, F. Ren, G. Yang, J. Kim, A. Kuramata, and S. J. Pearton, *Appl. Phys. Lett.* **112**(3), 032107 (2018).

²⁴M. E. Ingebrigtsen, A. Y. Kuznetsov, B. G. Svensson, G. Alfieri, A. Mihaila, U. Badstübner, A. Perron, L. Vines, and J. B. Varley, *APL Mater.* **7**(2), 022510 (2019).

²⁵P. Blood and J. W. Orton, *The Electrical Characterization of Semiconductors Majority Carriers and Electron States* (Academic Press, 1992).

²⁶A. Galeckas, A. Hallén, S. Majdi, J. Linnros, and P. Pirouz, *Phys. Rev. B* **74**(23), 233203 (2006).

²⁷I. L. Kolevator, B. G. Svensson, and E. V. Monakhov, *J. Appl. Phys.* **124**(8), 085706 (2018).